J|A|C|S ARTICLES

Published on Web 06/22/2010

Modeling, Preparation, and Characterization of a Dipole Moment Switch Driven by *Z*/*E* Photoisomerization

Alfonso Melloni,[†,■] Riccardo Rossi Paccani,[†] Donato Donati,[†] Vinicio Zanirato,*[,‡] Adalgisa Sinicropi,[†] Maria Laura Parisi,[†] Elena Martin,[||] Mikhail Ryazantsev,[§] Wan Jian Ding,[§,#] Luis Manuel Frutos,[○] Riccardo Basosi,[†] Stefania Fusi,[†] Loredana Latterini,[⊥] Nicolas Ferré,[▽] and Massimo Olivucci*[,†,§]

Dipartimento di Chimica, Università degli Studi di Siena, via Aldo Moro 2, I-53100 Siena, Italy, Dipartimento di Scienze Farmaceutiche, Università di Ferrara, via Fossato di Mortara 17-19, I-44100 Ferrara, Italy, Chemistry Department, Bowling Green State University, Bowling Green Ohio 43403, Departamento de Ingeniería Química y Química Física, Universidad de Extremadura Avenida de Elvas, E-06071 Badajoz, Spain, Centro di Eccellenza Materiali Innovativi Nanostrutturati and Dipartimento di Chimica, Università degli Studi di Perugia, via Elce di Sotto 8, I-06123 Perugia, Italy, College of Chemistry, Beijing Normal University, Beijing 100875, People's Republic of China, Laboratoire de Chimie Théorique et de Modélisation Moléculaire, UMR 6517-CNRS Université de Provence, Case 521-Faculté de Saint-Jérôme, Av. Esc. Normandie Niemen, 13397 Marseille Cedex 20, France, and Departamento de Química Física, Universidad de Alcalá, 28871 Alcalá de Henares, Madrid, Spain

Received August 23, 2009; E-mail: znv@unife.it; molivuc@bgnet.bgsu.edu

Abstract: We report the results of a multidisciplinary research effort where the methods of computational photochemistry and retrosynthetic analysis/synthesis have contributed to the preparation of a novel N-alkylated indanylidene−pyrroline Schiff base featuring an exocyclic double bond and a permanent zwitterionic head. We show that, due to its large dipole moment and efficient photoisomerization, such a system may constitute the prototype of a novel generation of electrostatic switches achieving a reversible light-induced dipole moment change on the order of 30 D. The modeling of a peptide fragment incorporating the zwitterionic head into a conformationally rigid side chain shows that the switch can effectively modulate the fluorescence of a tryptophan probe.

Introduction

We have recently shown that N-alkylated indanylidene−pyrroline (NAIP) Schiff bases provide a class of biomimetic switches that replicate different aspects of the *Z*/*E* photoisomerization of rhodopsin (i.e., the visual pigment of superior animals).[1,2] Below we report the results of a multidisciplinary effort where the methods of computational photochemistry and retrosynthetic analysis/synthesis have contributed to the preparation of the NAIP switch **1**, featuring a stable zwitterionic head. We show that, due to its large dipole moment, **1** may constitute the prototype of a generation of electrostatic switches achieving, at the single-molecule level, a light-induced dipole moment inversion on the order of 30 D.

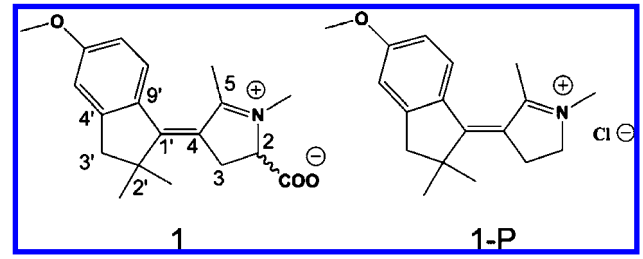

Photochemical switches (from now on "photoswitches") are bistable compounds that can be interconverted between two different isomers (states) via light irradiation. The most widely used photoswitch is azobenzene, which has been employed to control different biomolecular functions (see for instance refs 3−5). However, owing to the significant change in molecular length (ca. 3.5 Å between the two para carbons) but limited change in dipole moment (ca. 3 D) between its *Z* and *E* forms,[6] azobenzene is considered a mechanical rather than electrostatic

[†] Università degli Studi di Siena.
[‡] Università di Ferrara.
[§] Bowling Green State University.
[||] Universidad de Extremadura Avenida de Elvas.
[#] Beijing Normal University.
[○] Universidad de Alcalá.
[⊥] Università degli Studi di Perugia.
[▽] Université de Provence.
[■] Present address: Zambon Chemicals, via Davaro 2, I-36045 Almisano di Lonigo (VI), Italy.

(1) Sinicropi, A.; et al. *Proc. Natl. Acad. Sci. U.S.A.* **2008**, *46*, 17642–17647.
(2) Lumento, F.; Zanirato, V.; Fusi, S.; Busi, E.; Latterini, L.; Elisei, F.; Sinicropi, A.; Andruniòw, T.; Ferré, N.; Basosi, R.; Olivucci, M. *Angew. Chem., Int. Ed.* **2007**, *119*, 418–424.
(3) Harvey, J. H.; Trauner, D. *Chembiochem* **2008**, *9*, 191–193.
(4) Numano, R.; Szobota, S.; Lau, A. Y.; Gorostiza, P.; Volgraf, M.; Roux, B.; Trauner, D.; Isacoff, E. Y. *Proc. Natl. Acad. Sci. U.S.A.* **2009**, *106*, 6814–6819.
(5) Schierling, B.; Noël, A.-J.; Wende, W.; Hien, L. T.; Volkov, E.; Kubareva, E.; Oretskaya, T.; Kokkinidis, M.; Römpp, A.; Spengler, B.; Pingoud, A. *Proc. Natl. Acad. Sci. U.S.A.* **2010**, *107*, 1361–1366.
(6) Kumar, G. S.; Neckers, D. C. *Chem. Rev.* **1989**, *89*, 1915–1925.

10.1021/ja906733q

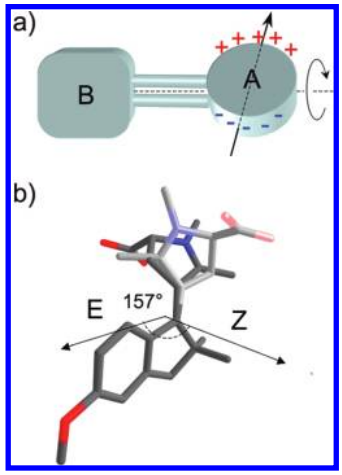

Figure 1. (a) Schematic representation of an electrostatic switch based on *Z*/*E* isomerization. The 180° rotation of unit A will invert the dipole moment vector with respect to unit B. (b) Inversion (relative to the superimposed indanylidene unit) of the dipole moment of S_0-*Z*-**1** and S_0-*E*-**1**. The computed dipole moment values are 15.7 and 14.8 D, respectively.

switch. Literature examples of electrostatic photoswitches are compounds of the spiropyran type that can be changed between a neutral state and a zwitterionic state via a photochemical ring-opening reaction. This property has been employed in different experiments to reversibly modulate the activity of enzymes[7−9] and channel proteins[10] and to achieve novel sensors.[11] Furthermore, it has been shown that the strong permanent dipole moment in the zwitterionic form of nitrospiropyran units attached to specific peptide residues is responsible for light-induced α-helix→random coil conformational transitions.[12]

In principle, the *Z*/*E* photoisomerization of olefins can provide the basis for the development of electrostatic photoswitches where a large dipole moment change is achieved via a ca. 180° rotation of a functionalized alkylidene unit. As shown in Figure 1a, the placement of opposite charges on unit A along an axis orthogonal to the central double bond provides a permanent dipole moment that is exactly inverted (with respect to unit B) upon double-bond isomerization. Note that, provided that the unit B is spatially constrained, the molecular dipole moment inverts sign rather than changes intensity (as in spiropyrans, where it goes from a small to a large value without direction control), leading to a maximum electrostatic potential change on the surrounding environment.

As a working hypothesis, we propose that a system of the type described above can be achieved via functionalization of the known NAIP photoswitch **1-P**.[2] The photochemical and spectral characterization of **1-P** (a chloride-alkylated Schiff base ion pair) in methanol reveals a prompt wavelength control of the *Z*/*E* photostationary composition as well as a *Z*→*E*→*Z* photocycle that is completed in ca. 20 ps.[1] The same studies also reveal that ab initio multiconfigurational quantum-chemical

Scheme 1. Retrosynthetic Analysis for the NAIP Schiff Bases **1-P** and **1**

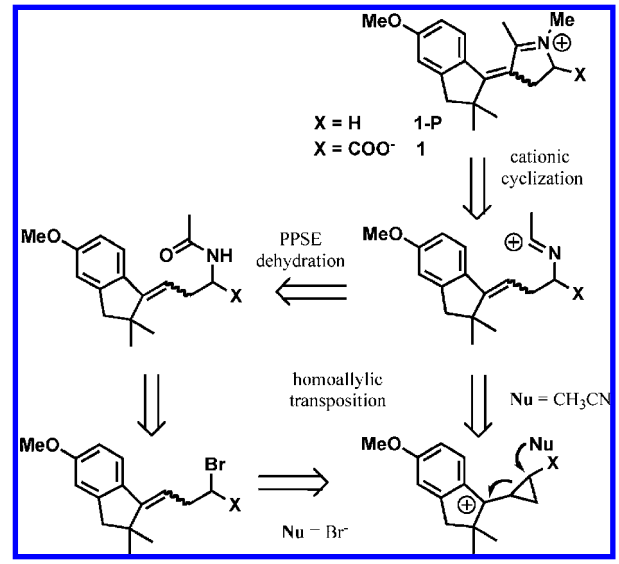

methods coupled with a molecular mechanics force field allow a realistic modeling of the excited states of the system as well as of other solution-phase NAIPs.

The zwitterion **1** is a derivative of **1-P** in which a nonconjugating internal carboxylate (replacing the external chloride) is substituted at C2. Nakanishi and co-workers[13] have reported the synthesis and characterization of different zwitterionic alkylated Schiff bases. These were used to investigate the point charge model for the control of the absorption wavelength in visual receptors. However, to our knowledge, **1** represents the first zwitterionic Schiff base where two relatively rigid frameworks (i.e., five-membered rings) are connected by a single exocyclic double bond, providing full conformational control.

In the following we report the result of a four-stage work starting with the construction and analysis of a quantum-mechanics/molecular-mechanics (QM/MM) model of **1**. Since the model indicates that **1** has the same favorable photochemical and spectral features as **1-P**, during the second stage of the work we design and perform the synthesis of a zwitterionic derivative. The characterization of the prepared compound shows that the predicted features are supported by spectral and photochemical data. Through the continuation of the synthesis work, we then show that **1-P** can be turned into an unnatural α-amino acid featuring a quaternary α-carbon at C2′. Finally, since the results above support the possibility of preparing semisynthetic proteins incorporating **1** as a rigidly oriented side chain, we build a QM/MM model of a tripeptide fragment incorporating a tryptophan probe. The simulation of the tryptophan emission maximum for the *Z* and *E* forms of the peptide is used to quantify the ability of the switch to control the optical properties of the fragment.

Methods

Synthesis. The synthesis of the zwitterionic switch **1** was accomplished using a procedure developed in our laboratories for the preparation of nonfunctionalized switches.[2,14] A cationic cyclization reaction of a transient nitrilium ion is the featured step leading to the indanylidene−pyrroline framework of **1-P**. As retrosynthetically depicted in Scheme 1, the homoallylic transposi-

(7) Hug, D. H.; O'Donnel, P. S.; Hunter, J. K. *Photochem. Photobiol.* **1980**, *32*, 841–848.
(8) Aizawa, M.; Namba, K.; Suzuki, S. *Arch. Biochem. Biophys.* **1977**, *180*, 41–48.
(9) Mayer, G.; Heckel, A. *Angew. Chem., Int. Ed.* **2006**, *45*, 4900–4921.
(10) Kocer, A.; Walko, M.; Meijberg, W.; Feringa, B. L. *Science* **2005**, *309*, 755–758.
(11) Fölling, J.; Belov, V.; Kunetsky, R.; Medda, R.; Schönle, A.; Egner, A.; Eggeling, C.; Bossi, M.; Hell, S. W. *Angew. Chem., Int. Ed.* **2007**, *46*, 6266–6270.
(12) Angelini, N.; Corrias, B.; Fissi, A.; Pieroni, O.; Lenci, F. *Biophys. J.* **1998**, *74*, 2601–2610.
(13) Sheves, M.; Nakanishi, K. *J. Am. Chem. Soc.* **1983**, *105*, 4033–4039.
(14) Zanirato, V.; Pollini, G. P.; De Risi, C.; Valente, F.; Melloni, A.; Fusi, S.; Barbetti, J.; Olivucci, M. *Tetrahedron* **2007**, *63*, 4975–4982.

Scheme 2. Synthetic Strategy Used To Obtain the Molecular Zwitterionic *Z*-**1**[a]

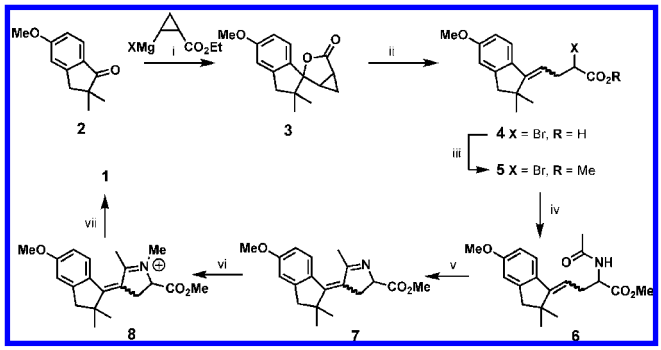

[a] Reagents and conditions: (i) ethyl 2-iodocyclopropanecarboxylate, iPrMgCl (54%); (ii) HBr/AcOH (95%); (iii) Me_3SiCHN_2 (91%); (iv) (a) NaN_3−DMF, (b) Ph_3P−H_2O, (c) AcCl Et_3N (65%, three steps); (v) PPSE (46%); (vi) MeOTf (98%); (vii) LiOH (53%).

tion of cyclopropylindenylcarbenium triggered by the bromide or, alternatively, by CH_3CN was the key step on the route to the pivotal electrophilic nitrilium ion. Thus, it was conjectured that **1** could be obtained by triggering the rearrangement of the proper carboxyl-functionalized cyclopropylindenylcarbenium intermediate.

The homoallylic rearrangement[15] has been widely exploited to install a 3-bromopropenyl side chain onto different substrates by reacting unsubstituted as well as aryl- or alkyl-substituted cyclopropylcarbinols with HBr. Instead, to our knowledge, only in a few cases[16−18] has the reaction been extended to carboxyl-functionalized cyclopropylcarbinols. Moreover, it is known that a lack of regioselectivity in the bromide attack at the α-carboxy cyclopropyl carbon atom would lead unavoidably to a mixture of isomeric compounds.

As shown in Scheme 2, to begin the synthesis, we needed to add the functionalized cyclopropylmagnesium reagent to the already reported 5-methoxy-2,2-dimethylindan-1-one (**2**). The goal was achieved following the protocol recently introduced by Knochel,[19] entailing the metal−halogen exchange between *i*-PrMgCl and *cis*-2-iodocyclopropanecarboxylate followed by the in situ trapping of the organometallic reagent with electrophiles. Indeed, employing compound **2** as the electrophilic counterpart, the reaction went to completion with a spontaneous lactonization, giving the spiro compound **3**. We were delighted to find out that the latter, when treated with HBr/AcOH, underwent the crucial homoallylic rearrangement in a completely regioselective manner, the α-bromoindanylidene carboxylic acid **4** being the only isolable compound. Restoration of the ester group by treatment of the carboxyl derivative **4** (as a 3:1 mixture of *Z*/*E* isomers) with (trimethylsilyl)diazomethane allowed the facile installation of the tethered acetamido group. Thus, from the methyl ester **5**, following our reported synthetic sequence entailing bromide displacement with sodium azide, Staudinger reduction, and acetylation, we acceded the pivotal secondary amide for nitrilium ion generation. As expected, trimethylsilyl polyphosphate[20] (PPSE)-promoted dehydration of compound **6** led directly to the free imine **7**, which subsequently was transformed to the corresponding iminium triflate **8** by treatment with methyl triflate. At this stage, in order to get the zwitterionic compound, the methyl ester group was saponified with LiOH. From the crude product taken up in acetonitrile we could precipitate the lithium triflate; after that the soluble fraction containing the zwitterion was purified by silica gel column chromatography. The targeted zwitterionic switch **1** was then isolated.

Scheme 3[a]

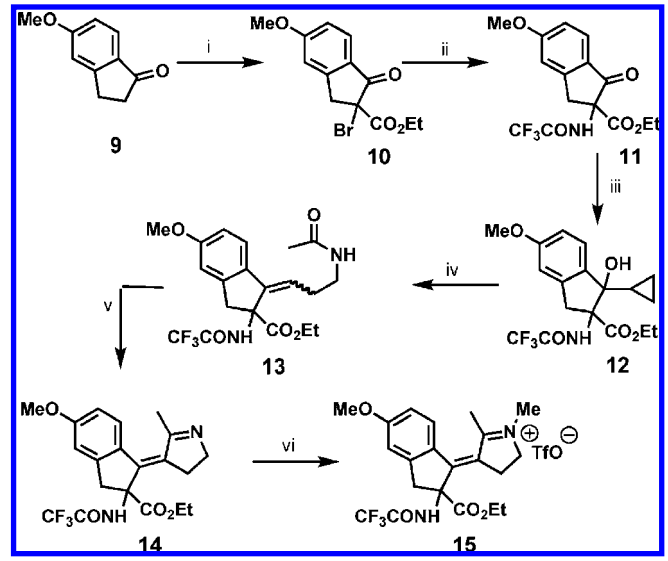

[a] Reagents and conditions: (i) (a) NaH, $(EtO)_2CO$, (b) NBS (90%); (ii) (a) NaN_3, (b) Ph_3P, (c) $(CF_3CO)_2O$ (90%); (iii) cPrMgBr (78%); (iv) Tf_2O, CH_3CN (81%); (v) PPSE (63%); (vi) MeOTf (95%).

In order to demonstrate that the parent switch **1** can be incorporated in an unnatural α-amino acid featuring a conformationally locked side chain, we have also carried out the synthesis of compound **15** (Scheme 3). This is a derivative of **1-P** where protected amino and carboxylic functions have been inserted in position C2′. The preparation of **15** required the indanone derivative **11** as the key starting material, which was easily obtained from the commercially available 5-methoxy-1-indanone (**9**) through functionalization of the C2 carbon atom. In detail, the synthesis commenced with the ethoxycarbonylation and α-bromination reactions to give compound **10**. The subsequent nitrogen introduction was achieved via bromide displacement with sodium azide, Staudinger reduction, and trifluoroacetylation of the resulting primary amine. We could ascertain the structure of the suitably protected α-amino acid **11** by crystallographic data (CCDC 752436).

Having in hand the required indanone moiety, the stage was set to accede one pot to the NAIP precursor **14** by submitting the Grignard adduct **12** to the cyclopropyl ring-opening/nitrilium ion ring-closing tandem reaction.[14] Unexpectedly, treatment of cyclopropyl indanol **12** with triflic anhydride in the presence of acetonitrile led to compound **13**, compelling us to put into practice the alternative way of producing electrophilic nitrilium ion. Thus, PPSE-promoted dehydration of the secondary amide **13** followed by in situ cationic cyclization yielded the expected free base **14** that, in turn, provided the photoswitchable amino acid **15** after quaternization with methyl triflate. Further details of the synthesis of Scheme 3 will be published in a separate report.

Spectroscopy and Photochemistry. Photoisomerization was carried out with a 900 W irradiator and an *f*/3.4 monochromator (Applied Photophysics) apparatus and was followed by ^{1}H NMR spectroscopy (Bruker AC 200 and 400 spectrometers at 200.13 and 400.13 MHz, respectively). The composition of the photostationary state at different irradiation wavelengths was evaluated from the area ratio of the signal of the aromatic proton in the ortho position with respect to the exocyclic double bond (see above and the Supporting Information). UV/vis measurements were performed by using a Hewlett-Packard 8423 spectrophotometer. See the Supporting Information for further details.

Computations. The model of the *Z* and *E* switches in solution was constructed by placing the chromophore in a rectangular box

(15) Julia, M.; Julia, S.; Guégan, R. *Bull. Soc. Chim. Fr.* **1960**, 1072–1079.
(16) Stoemer, F.; Schenk, F.; Buschmann, H. *Chem. Ber.* **1928**, *61*, 2312–2323.
(17) Stoermer, R.; Keller, W. *Chem. Ber.* **1931**, *64*, 2783–2792.
(18) Julia, M.; Mouzin, G.; Descoins, C. *C. R. Chim.* **1967**, *264*, 330–332.
(19) Vu, V. A.; Marek, I.; Polborn, K.; Knochel, P. *Angew. Chem., Int. Ed.* **2002**, *41*, 2535–2538.
(20) Gawley, R. E.; Chemburkar, S. R. *Heterocycles* **1989**, *29*, 1283–1292.

Scheme 4. QM/MM Model of Ala-**Zw**-Trp

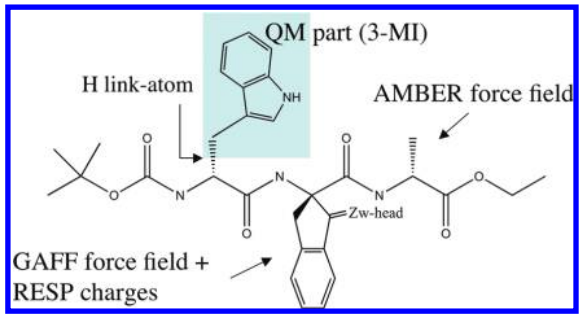

of methanol molecules positioned within 10 Å from any given atom of the chromophore by using the xleap module of the Amber package.[21] The average ground-state configuration of the methanol molecules (that is, the solvent) was determined according to the following procedure. The solvent was relaxed by 1000 conjugate-gradient minimization steps using periodic boundary conditions while keeping the chromophore (i.e., the solute) fixed in its gas-phase configuration. In this step the partial charges of the chromophore atoms were determined with GAUSSIAN03,[22] using a restrained electrostatic potential (RESP) procedure[23] at the HF/6-31G* level of theory. The minimized system was further relaxed (keeping the solute molecule fixed) using molecular dynamics simulation within an isothermal−isobaric NPT ensemble (1 atm, 298 K) using the program NAMD.[24] In the next step we performed CASSCF/6-31G*/AMBER geometry optimization to relax the coordinates of the QM chromophore and of all solvent molecules featuring at least one atom less than 4.5 Å away from any solute atom. The positions of the remaining solvent molecules, more distant from the chromophore, were kept frozen. The QM calculations were based on a CASSCF/6-31G* level, including an active space of 12 electrons in 11 π orbitals (that is, the full π system of the solute).

The chosen 6-31G* basis set represented a cost/accuracy compromise, yielding an excitation energy error of less than 3 kcal mol^{-1} for rhod and solution-phase PSB11.[25] CASSCF/6-31G*/AMBER geometry optimization was carried out with GAUSSIAN03[22] and TINKER 4.2.[26] To account for dynamic correlation energy, four root-state average CASPT2 calculations were carried out by using the MOLCAS 6.7[27] software. The quality of the achieved CASSCF/6-31G*/AMBER equilibrium structures was assessed by comparison with the structures computed using averaged solvent electrostatic potential/molecular dynamics (ASEP/MD) computations.[28] As we explain below and in the Supporting Information, this method, although computationally expensive, represents the best QM/MM-based method available for producing equilibrium structures by minimizing the Gibbs free energy.

The QM/MM model of the gas-phase tripeptide Ala-**Zw**-Trp (Scheme 4) was constructed using the CASSCF(10,9)/6-31G* QM level to describe the 3-methylindole (3-MI) fluorescent moiety of the Trp residue and the generalized amber force field (GAFF)[29] point charges to describe the rest of the peptide at the MM level including the unnatural **Zw** residue (see Results and Discussion). Accordingly, the QM/MM frontier was set at the weakly polarized $C_\alpha-C_\beta$ bond of Trp. The hydrogen link atom (HLA) scheme was used to saturate the QM C_β atom. The HLA was fixed at 1.0 Å from C_β and along the $C_\alpha-C_\beta$ bond axis. In order to avoid overpolarization of the QM wave function by the close point charges, the charge of the frontier C_α carbon atom was set to zero, and the charges of the other MM atoms of Trp were modified, since Trp is a natural residue (Table 1). This procedure is allowed by the small values of the original AMBER99 point charges, which also make it possible to use the standard MM van der Waals and bonded potentials parameters. The point charges of all other MM atoms (except those of the standard Ala residue) were determined via HF/6-31G* RESP calculations.

Table 1. Modified MM Point Charges for the Part of the Trp Residue (−NH−C_αH−CO−) That We Treated at the MM Level

atom	N	C_α	$C_{carbonyl}$	H_N	$O_{carbonyl}$	H_α
charge	−0.4157	0.0000	0.5973	0.24335	−0.5679	0.08375

As for the solution system described above, the QM/MM calculations were carried out with a modified version of GAUSSIAN03,[22] linked with a modified version of TINKER4.2.[26] The putative structures were drawn in two conformations (Conf1 and Conf2) that allowed a stabilizing stacking interaction between the **Zw** and Trp side chains and hydrogen bonding between the $-COO^-$ function of the Z form of **Zw** and the N−H group of the 3-MI moiety. The corresponding equilibrium structures were computed via QM/MM geometry optimization. On the basis of the QM/MM optimized ground-state (GS) structure, a CASPT2 single-point calculation was conducted with MOLCAS 6.7[27] to evaluate the excitation energies as well the associated oscillator strength *f*. The emission energies from the second excited state (that corresponds to the emitting ^{1}La state) were estimated by computing the GS−^{1}La vertical energy gaps via CASPT2 computations using a zeroth-order three-root state-average CASSCF wave function at the ^{1}La equilibrium geometry.

Results and Discussion

Recently[25,30] we implemented the ab initio CASPT2//CASSCF protocol (where equilibrium geometries and electronic energies are determined at the CASSCF[31] and CASPT2[32] levels, respectively) in a QM/MM scheme allowing for the evaluation of the excitation and emission energies of neutral or charged chromophores (treated quantum mechanically) embedded in protein or solution environments (described by the AMBER force field) with a few kcal mol^{-1} errors. Using this ab initio CASPT2//CASSCF/AMBER protocol, we were able to show[1,2] that the observed absorption and fluorescence maxima of **1-P** can be reproduced within a few kcal mol^{-1}. In the following the same methodology is used to achieve a description of the excited state (e.g., vertical excitation energy, nature of the spectroscopic state, geometric relaxation) of **1** in methanol solution.

In Table 2 we report the computed absorption maxima for the equilibrium S_0 structure of both the *Z* and *E* isomers of **1** (S_0-*Z*-**1** and S_0-*E*-**1** in Figure 2a). Consistent with the oscillator

(21) Case, D. A.; et al. *Amber 7*; University of California: San Francisco, 2002.
(22) Frisch, M. J.; et al. *GAUSSIAN03*, Revision B.04; Gaussian, Inc.: Pittsburgh, PA, 2003.
(23) Bayly, C. I.; Cieplak, P.; Cornell, W. D. *J. Phys. Chem.* **1993**, *97*, 10269–10280.
(24) Phillips, J. C.; Braun, R.; Wang, W.; Gumbart, J.; Tajkhorshid, E.; Villa, E.; Chipot, C.; Skeel, R. D.; Kale, L.; Schulten, K. *J. Comput. Chem.* **2005**, *26*, 1781–1802.
(25) Andruniow, T.; Ferré, N.; Olivucci, M. *Proc. Natl. Acad. Sci. U.S.A.* **2004**, *101*, 17908–17913.
(26) Ponder, J. W.; Richards, F. M. *J. Comput. Chem.* **1987**, *8*, 1016–1024.
(27) Andersson, K.; et al. *MOLCAS 6.7*; Lund University: Lund, Sweden, 2002.
(28) Sánchez, M. L.; Martín, M. E.; Galván, I. F.; Olivares del Valle, F. J.; Aguilar, M. A. *J. Phys. Chem. B* **2002**, *106*, 4813–4817.
(29) Wang, J.; Wolf, J. W.; Caldwell, R. M.; Kollman, P. A.; Case, D. A. *J. Comput. Chem.* **2004**, *25*, 1157–1174.
(30) Ferré, N.; Olivucci, M. *J. Am. Chem. Soc.* **2003**, *125*, 6868–6869.
(31) Roos, B. O. In *Ab Initio Methods in Quantum Chemistry-II*; Lawley, K. P., Ed.; Advances in Chemical Physics *69*; Wiley: New York, 1987; pp 399−446.
(32) Andersson, K.; Malmqvist, P.-A.; Roos, B. O.; Sadlej, A. J.; Wolinski, K. *J. Phys. Chem.* **1990**, *94*, 5483–5488.

Table 2. CASPT2//CASSCF/AMBER Absorption (λ_{max}), Change in Dipole Moment ($\Delta\mu$), Oscillator Strength (f), and Charge Translocation (Δq) Values

structure	exc	λ_{max} (nm)	$\Delta\mu$ (D)	f^a	Δq^b (au)
S_0-*Z*-**1**	$S_0 \rightarrow S_1$	390	9.4	0.646	−0.29
	$S_0 \rightarrow S_2$	304	0.8	0.026	−0.02
	$S_0 \rightarrow S_3$	250	1.1	0.210	−0.03
S_0-*E*-**1**	$S_0 \rightarrow S_1$	371	10.0	0.667	−0.27
	$S_0 \rightarrow S_2$	301	0.8	0.033	−0.02
	$S_0 \rightarrow S_3$	248	1.5	0.255	−0.04

[a] Oscillator strengths are calculated using the CASSCF zeroth-order wave function and CASSCF energies. [b] Charge transfer from the pyrroline to the indanylidene ring for **1** in MeOH.

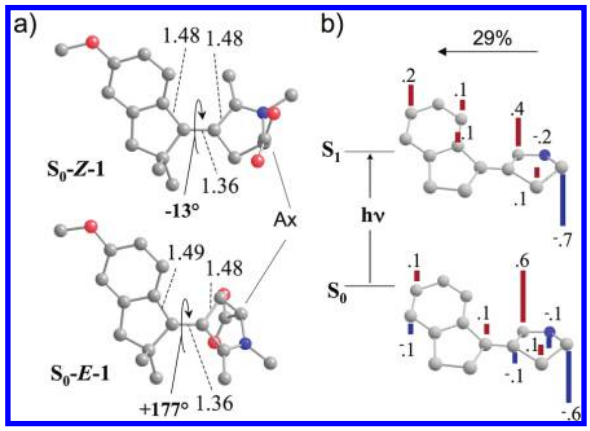

Figure 2. (a) CASSCF/AMBER computed equilibrium structures (hydrogens not shown) of S_0-*Z*-**1** and S_0-*E*-**1** embedded in a box (not shown) of methanol molecules. The computations are carried out for the *R* enantiomer and show that the $-COO^-$ group is stable in an axial (Ax) rather than an equatorial position in both forms (the equatorial positions appear to be unstable in methanol). The values in degrees refer to the C9′−C1′−C4−C5 torsional angle. Gas-phase and preliminary solution computations indicate that these values correspond to lowest energy conformations. (See also below. Solution conformations may exist with a C9′−C1′−C4−C5 torsional angle of opposite sign. These conformers will be investigated in a future work.) Bond lengths are given in Å. (b) Change in the charge distribution for the S_0-*Z*-**1** structure upon $S_0 \rightarrow S_1$ excitation.

strength values, the spectroscopic state corresponds to S_1. Figure 2b gives the S_0 and S_1 charge distribution computed for the ground-state equilibrium structure S_0-*Z*-**1**, which points to the charge-transfer nature of the spectroscopic state. Accordingly, upon $S_0 \rightarrow S_1$ vertical excitation, S_0-*Z*-**1** undergoes a 29% charge translocation through its reactive C1′═C4 bond from the pyrroline to the indanylidene moiety. On S_1 the positive charge is stabilized in a region away from the Schiff base function (C5═N) by delocalization on the phenyl ring. As found for the parent photoswitch **1-P**,[2] the electron-releasing *p*-OMe group further enhances the positive charge stabilization in the indanylidene moiety.

In Figure 3a, we report the relative CASPT2//CASSCF/AMBER energies for S_0-*Z*-**1** and S_0-*E*-**1** and for two associated S_1/S_0 conical intersections (CI-*Z*-**1** and CI-*E*-**1**) as a function of the torsional deformation along the reactive C1′═C4 bond. Similar to the case for the **1-P** ion pair,[2] we have located two very shallow (actually unstable) S_1 energy minima (S_1-*Z*-**1** and S_1-*E*-**1**) describing the region of the excited-state energy surface reached immediately after relaxation from the corresponding Franck−Condon points. In other words, CI-*Z*-**1** is located at the bottom of an initially flat S_1 potential energy surface valley reached via relaxation of the S_0-*Z*-**1** structure and developing out of the S_1-*Z*-**1** region. This is demonstrated in Figure 3b, which incorporates the result of intrinsic reaction coordinate (IRC) calculations starting at S_0-*Z*-**1** and reaching CI-*Z*-**1** after a barrierless path. Similarly, the second conical intersection is located at the bottom of the S_1 valley starting at S_1-*E*-**1**. As for **1-P**,[2] these structures are analogues of the excited-state minimum and conical intersection reported for the visual pigment rhodopsin (**Rh**).[25] While the S_1 energy surface always has a dominating charge-transfer character, at S_1-*Z*-**1** the S_1-S_2 energy gap is ≥ 10 kcal mol^{-1}. Therefore, it is consistent with a weak coupling between S_1 and the diradical (dark) state S_2.

The data in Figure 3a suggest, for both the *Z*→*E* and *E*→*Z* reactions, an isomerization mechanism (see full arrows for the *Z*→*E* process) similar to that fully documented for **1-P**[1] and **Rh**.[25] After $S_0 \rightarrow S_1$ photoexcitation, **1** initially relaxes along an S_1 path dominated by double-bond/single-bond inversion and only a limited torsional deformation. This initial event is followed by a torsional relaxation about the C1′═C4 bond. Indeed, upon excitation of the S_0-*Z*-**1** structure, which has a −13° pretwisted exocyclic C1′═C4 bond, it relaxes to an S_1-*Z*-**1** structure featuring an inverted π-bond order and a −20° twisted C1′═C4 bond. From the S_1-*Z*-**1** structure, the system evolves toward the conical intersection *Z*-**1**-CI, which is approximately −80° twisted (in the modeled *R* enantiomer), and it is accessed through a substantially barrierless path. After $S_1 \rightarrow S_0$ decay at the conical intersection, the S_0-*E*-**1** photoproduct (featuring a +177° pretwisted C1′═C4 bond) can be reached via further torsional relaxation in the same direction. At this point a photocycle can be achieved via subsequent photoisomerization of S_0-*E*-**1** (dashed arrows in Figure 3). Indeed, the data presented in Figure 3a support the existence of an S_0-*E*-**1** excited-state energy surface similar to that of S_0-*Z*-**1** and leading to S_1 evolution toward the *E*-**1**-CI intersection featuring an approximately 90° twisted C1′═C4 bond.

Similar to what was done for the parent compound **1-P**, the relative stability of S_0-*Z*-**1** and S_0-*E*-**1** in solution has been determined in terms of the difference in Gibbs free energy between the solvated systems using averaged solvent electrostatic potential/molecular dynamics (ASEP/MD) computations[28] (see the Supporting Information). The results indicate that, at 298 K, S_0-*E*-**1** is 4.1 kcal mol^{-1} higher in free energy than S_0-*Z*-**1**. This difference can be ascribed to steric hindrance factors; in fact, in the case of the *E* isomer the methyl substituent on C5 of the pyrroline ring is closer to the methyl substituents on C2′ of the indanylidene moiety. The larger difference in **1** relative to **1-P** could be due to diaxial interaction of the carboxylate and methyl groups.

As already mentioned above, **1** presents a permanent dipole moment that, with respect to the indanylidene unit, can be inverted via light-induced *Z*/*E* isomerization. The computed solution S_0 dipole moments are 15.7 and 14.8 D for the S_0-*Z*-**1** and S_0-*E*-**1**, respectively. As shown in Figure 1b, the superposition of the indanylidene units of the two isomers displays dipole moment vectors nearly orthogonal to the C1′−C4 axis and forming a 157° angle, thus yielding a difference module of 29.8 D. The dipole moment values, obtained within an explicit solvent representation (i.e., with a suitably constructed box of methanols), are confirmed by an implicit treatment of the solvent. Indeed, when using an independent solution model based on B3LYP/6-31+G* density functional theory with the polarizable continuum model (PCM) implemented in GAUSSIAN03,[22] the computed values of the S_0-*Z*-**1** and S_0-*E*-**1** dipole moments are 15.8 and 13.5 D, respectively. Therefore, both explicit and implicit solvent representations appear to yield large and consistent dipole moment values.

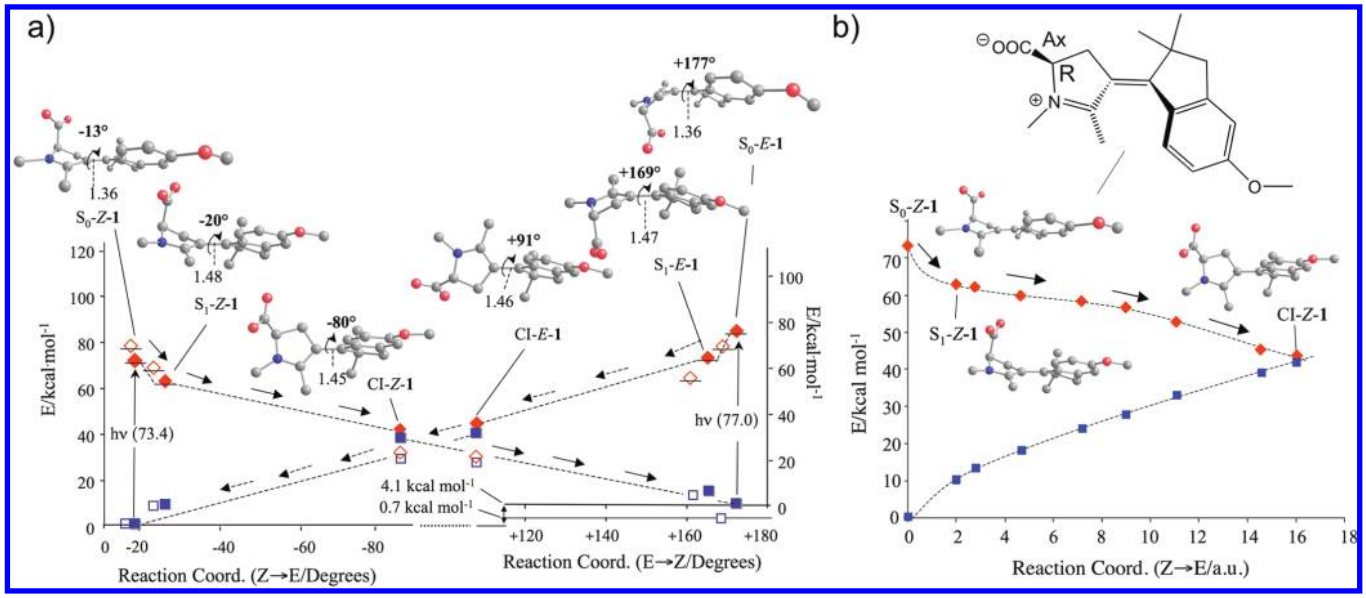

Figure 3. (a) S_1 (diamonds) and S_0 (squares) relative CASPT2//CASSCF/AMBER energies for the S_0, S_1, and CI points of **1** (solid symbols), characterizing its *Z*→*E*→*Z* photocycle in methanol solution. The energies of the corresponding **1-P** points (open symbols)[1] are also given for comparison. The structures (hydrogens not shown) provide a perspective showing the helicity of the molecular framework. The values in degrees refer to the C9′−C1′−C4−C5 torsional angle. Bond lengths are given in Å. Note that the difference between S_0-*E*-**1** and S_0-*Z*-**1** (and the corresponding **1-P** isomers) is calculated using averaged solvent electrostatic potential/molecular dynamics computations (see the Supporting Information). Note also that, due to the C2 stereogenic center, the ca. 90° twisted CI-*Z*-**1** and the CI-*E*-**1** structures are distinct distereoisomers that relax along stereochemically distinct S_0 paths connecting CI-*Z*-**1** to S_0-*E*-**1** and CI-*E*-**1** to S_0-*Z*-**1**. The ca. 40 kcal mol^{-1} gap between the S_0-*E*-**1** and S_0-*Z*-**1** equilibrium structures and the corresponding CI-*Z*-**1** and the CI-*E*-**1** is not related to the thermal isomerization barrier, which is smaller and requires the corresponding solvated transition structure to be evaluated. (b) S_1 energy profile (diamonds) along the computed S_1 IRC path for the *Z*→*E* photoisomerization of S_0-Z-**1**. It is shown that S_0-Z-**1**, S_1-Z-**1**, and CI-Z-**1** are connected by a barrierless reaction coordinate. The IRC value is given in atomic units (au, amu$^{1/2}$ bohr). The S_0 energy profile (squares) along the computed S_1 coordinate and the *M*,*M* helicity of the computed (*R*)-S_0-*Z*-**1** conformer are also shown. In the formula at the top, *R* indicates the absolute configuration of the C2 center and Ax the axial position of the −COO^- substituent.

Since the dipole moments of **1** could only be predicted and not measured, we benchmarked the employed computational methods indirectly. Using the B3LYP/6-31+G* and PCM methods, we have evaluated the dipole moments of **1** in dioxane, finding slightly decreased values with respect to methanol (13.7 and 11.6 D for the *Z* and *E* form, respectively). With exactly the same method, we also computed the dipole moments of an experimentally investigated merocyanine−spirobenzopyran system in dioxane and compared the results with the observed values available in the literature.[33] The observed dipole moments (17.7 and 4.3 D for the open merocyanine and closed spiropyran forms, respectively) compare reasonably well with the computed data (15.9 and 6.9 D, respectively), pointing to moderately underestimated predictions.

The computational evidence for an efficient photoisomerization, a ca. 30 D light-driven dipole moment change and, ultimately, the possibility to achieve a novel class of electrostatic switches, prompted the search for a viable preparation of **1**. The synthetic protocol adopted for the preparation of the parent compound **1-P** (see Scheme 1) involved establishing a polyconjugated iminium ion chromophore onto a rigid framework consisting of an indanylidene nucleus connected to a pyrrolinium ring.[2,14] As detailed in the Methods section and shown in Scheme 2, a cationic cyclization reaction of a transient nitrilium ion with an internal olefin was successfully employed as the key step in setting up the desired chromophore (for further details and full spectroscopic characterizations of the new compounds, see the Supporting Information).

As shown in Figure 4, the absorption spectra of *Z*-**1** and *E*-**1** in methanol display two bands absorbing above 250 nm. The

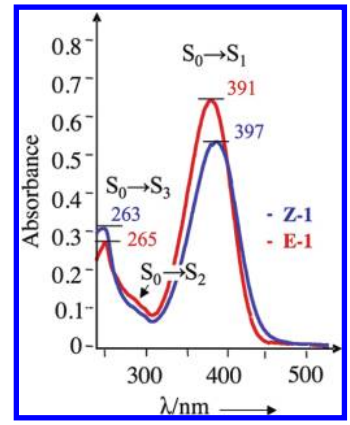

Figure 4. Room-temperature experimental absorption spectra of the *Z* isomer (blue line) and *E* isomer (red line) of **1** in MeOH.

observed λ_{max} values and intensities were compared with the predicted properties in Table 2 to validate our computational models and, in turn, to assign the bands to given electronic transitions. In fact, the computed S_0→S_1 absorption maximum for the *Z* isomer (λ_{max}) falls within 10 nm of the intense band at 397 nm, which yields a computational error of less than 2 kcal mol^{-1} in excitation energy.

Similarly, the observed weaker band at λ_{max} = 263 nm falls close to the computed S_0→S_3 transition. Furthermore, the S_0→S_1 and S_0→S_3 values of the oscillator strength *f* (0.646 and 0.210, respectively) are qualitatively consistent with the observed absorbance pattern. The S_0→S_2 transition is predicted to correspond to a weak band (f = 0.026) most probably hidden below the shoulder near 300 nm, as indicated in Figure 4.

(33) Bletz, M.; Pfeifer-Fukumura, U.; Kolb, U.; Baumann, W. *J. Phys. Chem. A* **2002**, *106*, 2232–2236.

The computational results displayed in Figure 3 indicate that S_0-*Z*-**1** and S_0-*E*-**1** can be photochemically interconverted via barrierless, and therefore ultrafast (i.e., with a time scale below 1 ps), reactions. This conclusion is in agreement with the results of a recently reported[34] combined femtosecond fluorescence up-conversion, UV−vis, and IR transient absorption spectroscopic study of **1**. Indeed, the fluorescence lifetime for the *Z*→*E* process is found to be 140 fs, with an excited-state absorption persisting over 230 fs in the form of a vibrational wavepacket according to twisting of the isomerizing double bond. It is also shown that the hot photoproduct appears at the ground state on a 400 fs time scale and that the reaction is substantially completed after 600 fs from photon absorption.

To assign the observed time scale, we have used a recently proposed computational strategy to simulate the excited-state motion of **1** in methanol. Accordingly, we computed a scaled CASSCF/AMBER trajectory[35] of our *Z*-**1** solvated model (i.e., the same used to reproduce the reaction path of Figure 3b) starting at a point close to the Franck−Condon structure and describing the relaxation of the first solvent shell together with the solute. In this calculation, the excited-state CASSCF gradient is scaled in such a way as to simulate the more accurate (but computationally impractical) CASPT2 gradient along the entire reaction path of Figure 3b. In other words such a trajectory simulates, at the cost of CASSCF gradients, the excited-state evolution on a CASPT2-like potential energy surface.[35] This protocol has reproduced successfully the magnitude of the observed excited-state lifetime of the retinal chromophore in **Rh** and provided a mechanism in line with its ultrafast isomerization.[35] Notice that it has not been possible to start the trajectory from the Franck−Condon structure due to the incorrect order (with respect to the corresponding CASPT2 values) of the S_2 and S_3 states computed at the CASSCF level of theory. The order becomes correct only at ca. 30° double bond twisting deformation (i.e., ca. 20° more twisted than the Franck−Condon structure). Thus, the computed trajectory provides an approximated lower limit of the reaction time scale that, according to Figure 5a and assuming a ca. 50 fs initial relaxation, is predicted to be in the 300−400 fs range. In spite of this uncertainty, the ultrafast nature of the isomerization and the magnitude of the predicted S_1 lifetime are consistent with the observed[34] excited-state dynamics that points to an excited-state lifetime between 250 and 400 fs. Notice that transient fluorescence is predicted to occur, assuming a ca. 50 fs initial relaxation time, during the first 200 fs as indicated by the values of the S_0−S_1 oscillator strength (see Figure 5a).

The scaled CASSCF/AMBER trajectory also reveals that the solvent cavity cannot stop the excited-state photoisomerization motion that, according to our analysis, is facilitated by the ring inversion of both the indanylidene and pyrrolinium envelope-like five-membered rings. Indeed, we could observe (see movie in the Supporting Information) an inversion of the axial/equatorial position of the two methyl and hydrogen groups at C2′ and C3, respectively. Because of the inversions, the double bond can undergo a twisting deformation of 90° and decay at the conical intersection without moving the bulkiest parts of the molecular framework. Indeed, as shown in Scheme 5, both the phenyl ring and the highly solvated $-COO^-$ and $N(Me)^+$ groups remain substantially fixed during the entire S_1 motion. The counterclockwise rotation about the reactive C1′−C4 double bond is accompanied by clockwise twisting (associated with

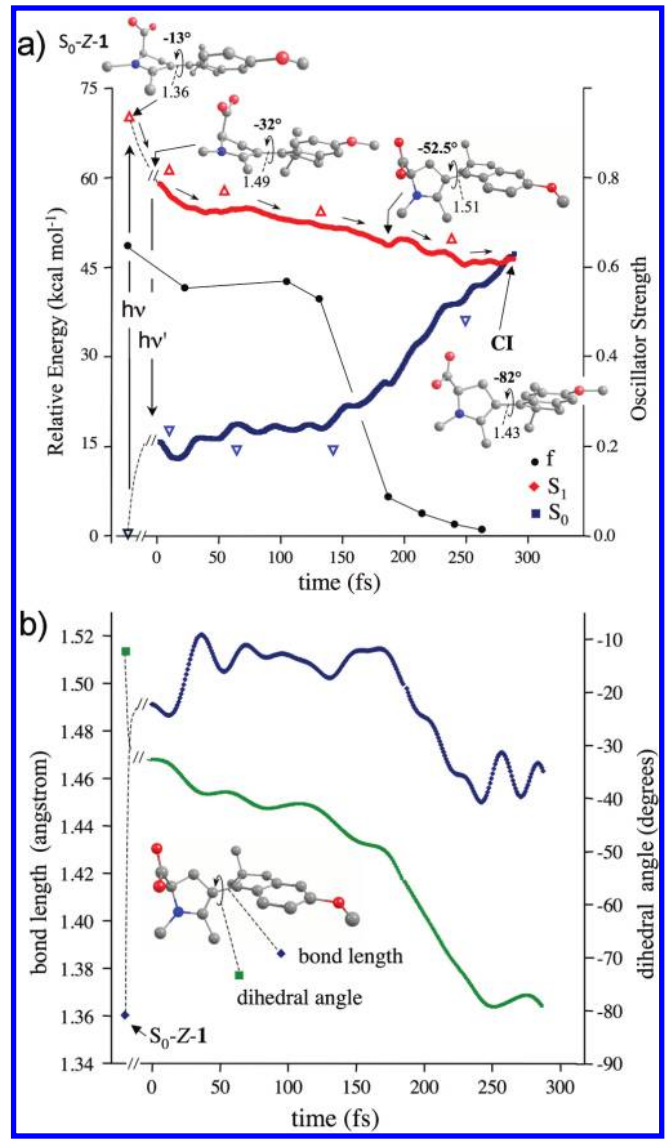

Figure 5. (a) Scaled CASSCF/AMBER trajectory simulating the S_1 isomerization of **1** in methanol solution. The system is predicted to reach the conical intersection region on a 300 fs time scale. The open triangles indicate single-point CASPT2//CASSCF/AMBER energies, demonstrating that the scaled CASSCF energy profile is only slightly off the CASPT2 energy. The CASSCF/AMBER value of the oscillator strength *f* along the trajectory is also given (full circles). (b) Evolution of the two main geometrical parameters (C1′−C4 length and C9′−C1′−C4−C5 dihedral) characterizing the S_1 structure of the switch.

Scheme 5. Conformational Changes Occurring during the Excited-State Trajectory of *Z*-**1** in Methanol and Allowing a Space-Saving Isomerization Motion[a]

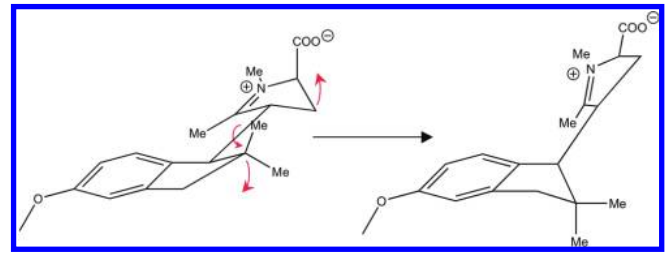

[a] See movie in the Supporting Information.

(34) Briand, J.; Bräm, O.; Réhault, J.; Léonard, J.; Cannizzo, A.; Chergui, M.; Zanirato, V.; Olivucci, M.; Helbing, J.; Haacke, S. *Phys. Chem. Chem. Phys.* **2010**, *12*, 3178–3187.

(35) Frutos, L. M.; Andruniów, T.; Santoro, F.; Ferré, N.; Olivucci, M. *Proc. Natl. Acad. Sci. U.S.A.* **2007**, *104*, 7764–7769.

Table 3. Composition of the Photostationary State of **1** in Methanol as a Function of the Irradiation Wavelength, Determined by NMR Analysis

λ_{max}^{abs} (nm)	*Z* (±0.1)	*E* (±0.1)
340	1	0.5
390	1	0.6
440	1	1.2

the ring inversion) of the C2′−C3′ and C2−C3 bonds. These directions are imposed by the pretwisting of the C1′−C4 double bond and initial ring conformation (i.e., imposing a framework with *M*,*M* helicity) of S_0-*Z*-**1** and, according to our computations, are a consequence of the system *R* configuration. This is reminiscent of the type of cooperative bond-twisting, space-saving mechanism documented for the retinal chromophore embedded in the chiral cavity of Rh.[35]

Since, according to Figure 3 and the experimental data presented in ref 34, both the Z→E and *E*→*Z* isomerizations are found to be ultrafast and the absorption λ_{max} values of *Z*-**1** and *E*-**1** are close but not identical (see Table 2), it is predicted that, upon continuous irradiation, a photostationary state will be rapidly generated whose composition depends on the irradiation wavelength, leading to the possibility to control the dipole moment value. Comparison of the *Z*-**1** and *E*-**1** spectra (see the Supporting Information) suggests, consistent with the computed λ_{max} data, a decrease of the *Z*/*E* ratio upon an increase in the wavelength (Table 3), since the $S_0 \rightarrow S_1$ band of *E*-**1** appears to be slightly blue-shifted and more intense than the corresponding *Z* band. In particular, at 440 nm, the *E* form becomes dominant. On the other hand, due to a relatively low *E*→*Z* thermal isomerization barrier, which has not yet been measured or computed, the photogenerated ratio slowly returns to the original *Z*/*E* mixture (a *Z*/*E* ratio larger than 99:1) when the irradiation is interrupted at room temperature (see the Supporting Information). This is consistent with the more than 4 kcal mol^{-1} computed energy difference between S_0-*Z*-**1** and S_0-*E*-**1**. Notice that, while the photostationary state is rapidly reached (e.g., 12 min irradiation at the isosbestic point), this room-temperature thermal relaxation/interconversion is not a fast process.

A relaxation time of about 8 h could be estimated, allowing the isomers to be fully characterized (see the Supporting Information for details). The systems could undergo irradiation−dark relaxation cycles several times without showing any degradation. This indicates that **1** can indeed be employed in applications where the photoswitch triggers molecular events that are completed on a time scale shorter than a few hours or when one wants to recover the original *Z*/*E* composition (and be ready to repeat a photoswitching cycle) after several hours or more. On the other hand, the 8 h relaxation time points to a thermal isomerization barrier smaller than the one expected for a C=C double bond. The origin of this low barrier is currently under investigation in our laboratory. The similarity between the reaction path in Figure 3 and that of the parent NAIP photoswitch and rhodopsin suggests that *Z*-**1** and *E*-**1** could potentially display good photoisomerization quantum yields. These quantities were measured via HPLC and spectroscopic analysis and found to be 0.20 and 0.23 for the *Z*-**1** and *E*-**1** isomerizations, respectively. The *E*→*Z* quantum yield was determined by considering the effect of the thermal *E*→*Z* isomerization on the isomer concentrations determined by HPLC. The fact that an ultrafast reaction driven by a barrierless path leads to a moderate quantum yield points to a decay mechanism that deviates from the simple one-dimensional Landau−Zener picture.[36] This could be connected with the multimode nature of the excited-state reaction path, involving both ring puckering and bond twisting, and/or with the restrains imposed, after the excited-state decay, by the solvent shell on the isomerization motion. Furthermore, the limited magnitude of the quantum yields may be related to the fact that, immediately after the S_1 decay and during the S_0 relaxation, the system needs to reshape the solvent shell to accomplish full double bond isomerization.

The successful photoisomerization documented above for **1** and the successful synthesis of the unnatural amino acid **15** (in a protected form), featuring a photoswitchable side chain, strongly support the possibility to achieve semisynthtetic peptides and proteins incorporating a dipole switch in a conformationally locked orientation. While we expect that the photoisomerization dynamics of these systems will differ from the dynamics calculated/observed for *Z*-**1** in methanol, the results above point to a facile process. More specifically, these achievements indicate that the amino acid **Zw** of Figure 6a is a realistic synthesis target that, in principle, only requires the tuning of the chemistry seen in Schemes 2 and 3. While the preparation of such a system goes beyond the scope of the present research, below we report on the computational design of a tripeptide (Ala-**Zw**-Trp) that incorporates **Zw** as the central residue and tryptophan as the N-terminal residue. The tryptophan residue constitutes an internal fluorescence probe sensing the changes in the electrostatic field produced in its environment. By virtue of the fact that **15**, and therefore **Zw**, features a quaternary α-carbon, the side chain of this residue is conformationally rigid and has a well-defined orientation with respect to the peptide backbone. In particular, as displayed in Figure 6b (right), this side chain would be orthogonal to the local backbone axis and is positioned off to the left or to the right of the same axis as a function of the stereochemistry (*R* or *S*) of the α-carbon.

Here our target is to assess if the *Z*/*E* photoisomerization reversing the dipole moment of the central residue would significantly change the tryptophan emission wavelength. In other words, we want to find out if the dipole moment inversion would expose the 3-MI fluorophore of tryptophan to a different electrostatic field, thus modulating its GS−^{1}La energy gap. In fact, as shown in Figure 6b, the fluorescent ^{1}La state of tryptophan has a charge-transfer character (ca. 30% of the pyrrole ring π-electron density is shifted toward the phenyl ring upon photoexcitation).[37] As a consequence, an electrostatic potential that stabilizes a positive charge on the 3-MI pyrrole ring or a negative charge on the phenyl ring will stabilize the ^{1}La state with respect to the GS, leading to a red shift of the fluorescence λ_{max}.

In the following the tripeptide is assumed to represent a fragment of the interior of a protein that is not in contact with the solvent; therefore, the calculations are carried out using isolated models (i.e., no solvent molecules are considered). As displayed in Figure 6, we have investigated one stereoisomer of the switch (the configuration of the C2′ quaternary α-carbon of **Zw** is *R* and the configuration of the C2 carbon is *S*), allowing for a shorter distance between the **Zw** and Trp residues. We consider (see the Supporting Information for details) two specifically designed conformers (Conf1-Ala-**Zw**-Trp and Conf2-

(36) Desouter-Lecomte, M.; Lorquet, J. C. *J. Chem. Phys.* **1977**, *66*, 4006–4017.
(37) Pistolesi, S.; Sinicropi, A.; Pogni, R.; Basosi, R.; Ferreé, N.; Olivucci, M. *J. Phys. Chem. B* **2009**, *113*, 16082–16090.

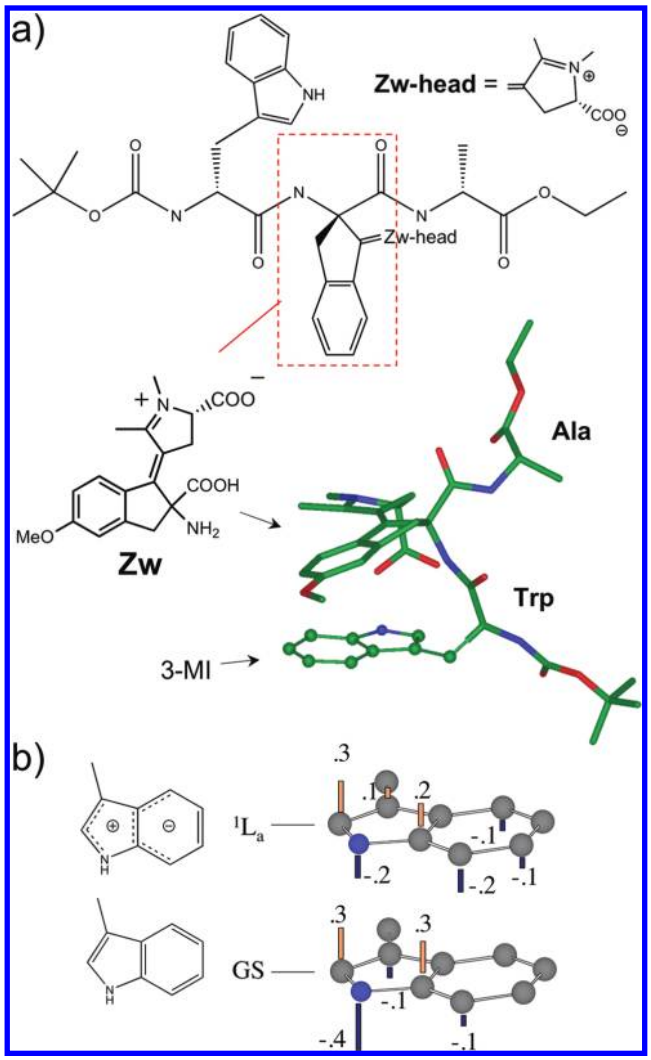

Figure 6. (a) Structure of the designed Ala-**Zw**-Trp tripeptide. The incorporated unnatural amino acid **Zw** is framed. The position of the 3-MI fluorophore (ball-and-stick representation) treated at the QM level with respect to the peptide backbone and to the rigidly oriented zwitterionic side chain of the **Zw** residue (tube representation) of Conf1-Ala-**Zw**-Trp is shown. (b) The ground-state (GS) and fluorescent-state (^{1}La) charged distribution of 3-MI from ref 37.

Ala-**Zw**-Trp) of the stereoisomer, both featuring stacked and hydrogen-bonded Trp and **Zw** side chains (the *Z* forms of Figure 7). This situation is reminiscent of the documented Arg-Trp stacking documented for cytokine-binding proteins[38] where, loosely, the positively charged arginine unit is replaced by the pyrrolinium moiety.

Conf1 features an extended backbone, while Conf2 has a β-turn-like backbone. As mentioned above, Conf1-Ala-**Zw**-Trp and Conf2-Ala-**Zw**-Trp are assumed to represent different realistic arrangements of the chosen tripeptide fragment in a protein. The effect of the photoisomerization on the tryptophan fluorescence is determined in the following way. The structure of the corresponding fluorescent conformers (i.e., featuring the 3-MI moiety in its ^{1}La state) is optimized at the CASSCF/6-31G*/AMBER QM/MM level. Accordingly, the QM part corresponds to the 3-MI side chain of tryptophan, while the rest of the molecule is described at the MM level (see Methods section for details). The central residue corresponding to the unnatural amino acid **Zw** and the Ala residue are described at the MM level with a GAFF potential and features parametrized RESP charges (computed at the HF/6-31G* level) for both the *Z* and *E* forms.

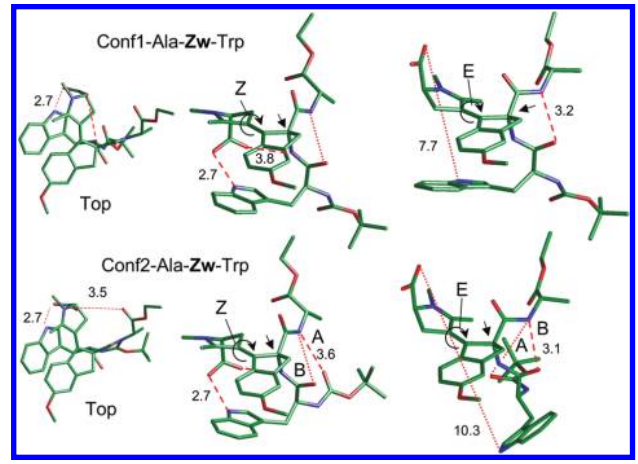

Figure 7. Structure of the designed Ala-**Zw**-Trp tripeptide in its fluorescent state (i.e., at the ^{1}La equilibrium geometry). The incorporated unnatural amino acid **Zw** is in its *R* configuration (see straight arrow), while the $-COO^-$ group resides on an asymmetric carbon with *S* configuration. The curly arrows indicate the position of the isomerizing double bond. The hydrogen bonds present in the structures are indicated with dashed lines. The incipient or broken hydrogen bonds are indicated with dotted lines. The distances are given in Å. The labels A and B facilitate the reading of the hydrogen-bonding change in Conf2.

Table 4. Computed Fluorescence Maxima (λ^{fl}_{max}) for the Conf1 and Conf2 Conformers of the Ala-**Zw**-Trp Tripeptide and for the Gas-Phase Fluorophore 3-MI (from ref 37)[a]

	ΔE (kcal mol^{-1})[b]	λ^{fl}_{max} (nm)	*f*	$\Delta\mu$ (D)
3-MI	97.1	295	0.11	5.9
Z-Conf1	90.0 (96.4)	318	0.10	5.2
E-Conf1	98.5 (97.3)	290	0.11	4.9
Z-Conf2	91.9 (96.5)	311	0.11	5.2
E-Conf2	100.0 (98.0)	286	0.12	4.8

[a] The active space used in the calculation comprises the full π-system of the 3-MI fluorophore. The oscillator strength (*f*) and the change in the dipole moment ($\Delta\mu$) upon the vertical electronic transition are also given. [b] Values in parentheses were calculated in the absence of MM point charges of the models; see text.

The energy gaps between the fluorescent state and the ground state are computed via CASPT2//CASSCF/6-31G*/AMBER single-point computations and correspond to the $S_0 \rightarrow S_2$ transition (the ^{1}La state features the largest oscillator strength with respect to the ground state). In Table 4 we show that, according to our QM/MM models, the tryptophan fluorescence can be modulated via $Z \rightarrow E$ photoisomerization. In particular, the Conf1-Ala-**Zw**-Trp and Conf2-Ala-**Zw**-Trp emissions are significantly blue-shifted (28 and 25 mm, respectively) upon photoisomerization. Notice that these effects correspond to an increase in the $S_0-{}^1$La energy gap of more than 8 kcal mol^{-1}. It is also remarkable to find out that the emission maxima of the *Z* and *E* forms are predicted to be respectively strongly red-shifted and blue-shifted with respect to that of the isolated 3-MI.

In order to demonstrate that the above changes are dominated by the different electrostatic field created by the change in orientation of the **Zw-head** moiety, we have repeated the energy gap calculation using the same ^{1}La equilibrium peptide structures in the absence of the MM point charges of the models, which are responsible for the electrostatic field acting on the fluorophore. The results of these calculations (see values in parentheses

(38) Bravo, J.; Staunton, D.; Heath, J. K.; Jones, E. Y. *EMBO J.* **1998**, *17*, 1665–1674.

in Table 4) fully confirm that the energy gap change is due to a change in electrostatics. Indeed, the resulting energy gaps are all within 1 kcal mol^{-1} of the corresponding isolated 3-MI value.

The results above can be readily explained considering the typical GS and ^{1}La charge distributions seen in Figure 6b as well as the geometry of the peptide conformers seen in Figure 7. In fact, both *Z*-isomers feature a hydrogen bond between the ionized $-COO^-$ group of the switch, placed directly above the 3-MI unit and the indole N−H bond. This situation would strongly stabilize the excited state with respect to the ground state due to the short distance between the $-COO^-$ negative charge and the pyrrole moiety positive charge of ^{1}La 3-MI. The removal of this interaction in both *E*-isomers must therefore lead to a blue-shift of the absorption due to a less stabilized ^{1}La state.

The analysis of the *E* and *Z* conformers also provide information on the possible structural effects induced upon photoisomerization and can be due to both mechanical (i.e., bond-breaking) and electrostatic changes. For instance, in Conf1-Ala-**Zw**-Trp the photoisomerization breaks the $-COO^-\cdots H-N$ hydrogen bond, which also results in the formation of an intra-backbone hydrogen bond stabilizing the conformer. Interestingly the breaking of the $-COO^-\cdots H-N$ hydrogen bond in Conf2-Ala-**Zw**-Trp leads, in our model, to a backbone rearrangement involving the breaking of the hydrogen bond A and the formation of the new hydrogen bond B shown in Figure 7.

Conclusions

The photoinduced dipole moment change of spiropyran−merocyanine electrostatic photoswitches has been measured for the case of indolino−spirobenzopyrans.[33] The results indicate a maximum dipole moment change of ca. 17 D due to the low dipole moment (ca. 3 D) of the spiropyran closed form with respect to the merocyanine open form (ca. 15 D). In a situation where the indanylidene ring is rigidly oriented, the presented NAIP Schiff base **1** provides an electrostatic photoswitch displaying a nearly 2-fold dipole change. This is due to the spatial inversion (reorientation) of a large (ca. 15 D) permanent dipole moment (see Figure 1).

The ca. 30 D dipole moment change of **1** opens up a new perspective for the light-driven conformational control of macromolecular structures determined by polar interactions. In a situation where the indanylidene ring is held in a fixed orientation (e.g., when part of a protein backbone or supramolecular scaffold), light can be used to invert the dipole, yielding a dramatic change in the local electrostatic field and, ultimately, a conformational change thus leading to a destabilization of the original equilibrium conformation. The construction of QM/MM models of the *Z* and *E* forms of the Ala-**Zw**-Trp tripeptide strongly supports this hypothesis. In fact, we have provided computational evidence that the Ala-**Zw**-Trp photoisomerization leads to easily detectable (>20 nm) changes in the fluorescence maximum, thus providing an excellent basis for future experimental work. Furthermore, given the presence of the charged carboxylate and imminium centers in the rotating head (**Zw-head** in Figure 6a), the same photoisomerization could be used to break and reconstitute hydrogen bonds and salt bridges in suitably designed peptides. However, as mentioned above, to implement these concepts one needs further functionalization of **1** at the level of the indanylidene ring (introducing, for instance, $-NH_2$ and −COOH groups) to graft the molecule to the macromolecule backbone. For instance, one could repeat the synthesis of Scheme 2 using the intermediate **11** rather than the substrate **2** as the indanone precursor. Synthesis work in this direction is currently being carried out in our laboratories.

A different perspective may be opened by the preparation of enantiomerically pure **1** (e.g., via chiral resolution of the available racemate). Similar to the well-known chiral diarylidenes, the *R* and *S* enantiomers of **1** display molecular helicity. According to our computation, the lowest energy solution conformers of *Z*-**1** and *E*-**1** have axial carboxylates and pretwisted double bonds in the same direction (clockwise). This establishes that the *R* (*S*) configuration at C2 induces an *M*,*M* (*P*,*P*) helicity (see Figure 3 for the case of the *R* enantiomer) in the lower energy diastereomeric conformer of both the *Z* and *E* forms. This leads to the possibility of a preferential direction of isomerization and, ultimately, to a two-photon-induced unidirectional rotary motion of the **Zw-head** with respect to the indanylidene unit. Indeed, the IRC of Figure 3b displays a clockwise rotation of the S_0-*Z*-**1** pyrrolinium head that would continue upon relaxation to the S_0-*Z*-**1** intermediate. Future computational work will explore this perspective.

Acknowledgment. We are grateful to Jan Helbing and Stefan Haacke for valuable discussions. This work was supported by the Università di Siena (PAR02/04), FIRB (RBAU01EPMR), COFIN2006 (Prot. 200431072_002), and Bowling Green State University. M.O. is grateful to the Center for Photochemical Sciences and the School of Arts & Sciences of Bowling Green State University for start-up funds. L.-M.F. acknowledges the financial support from a "Ramon y Cajal" contract and project CTQ2009-07120 of the Spanish MICINN.

Supporting Information Available: Details of the synthesis, QM/MM computations, ASEP/MD calculation, spectroscopy and photochemistry, and complete refs 1, 21, 22, and 27; a movie displaying the computed excited-state isomerization motion of *Z*-**1** in methanol solution (the solvation shell is displayed). This material is available free of charge via the Internet at http://pubs.acs.org.

JA906733Q